**Novel Filler Materials for Composite Out-of-Plane Joints**

Zsombor Sápi[a], Sam Hutchins[b], Richard Butler[a*], Andrew Rhead[a]

[a] Materials and Structures Research Centre, Department of Mechanical Engineering, University of Bath, Claverton Down, Bath, BA2 7AY, United Kingdom

[b] Composites Research Centre, GKN Aerospace, Ferry Rd, East Cowes, PO32 6RA, United Kingdom

**Abstract**

In the manufacture of the out-of-plane joints of composite stiffened panels, such as the connection between skin and T, I, omega shaped stiffeners, a filler material is needed to fill the void between the flanges, web and skin. The most common filler is a rolled unidirectional prepreg tape ("noodle"), which is not only expensive to manufacture, but also has low strength that can lead to premature failure of the loaded joint. In this work, eight novel filler concepts are introduced and experimentally validated against the baseline noodle via T-joint tensile tests. Polyamide nonwoven interleaved joints increase the damage tolerance of the structure and nonwoven nanofibres increase the failure initiation load. 3D printed fillers have lower strength but demonstrate the possibility of thermoplastic-thermoset hybrid structures. Fillers made of chopped prepreg match the strength of the baseline noodle and can serve as a low cost replacement. Another low cost, resin infused braided concept has lower strength, but its counterpart using multiple individual braids has the same strength as the unidirectional noodle. Moreover, the latter concept shows that different resin systems can be cured together

[*] Corresponding author. E-mail address: R.Butler@bath.ac.uk

without causing a knockdown in strength, and can serve as a basis for a range of novel applications.

**Keywords**

Noodle; T-joint; Stiffener; Stiffened panel; Deltoid

## 1. Introduction

Laminated composite materials possess great weight saving potential in many applications due to their high relative strength and stiffness. However, thin shell structures are prone to buckling and have low out-of-plane strength. As a reinforcement, stiffeners with various profiles can be attached to the laminate to form a stiffened panel requiring a transition of the in-plane loads to the weaker, out-of-plane direction. The most common sections used in aerospace structures are T, I, Z, L and hat (omega) stiffeners. The geometry and layup of these greatly define the buckling and post-buckling behaviour of the stiffened panel [1–3] and its tendency to avoid premature skin-stiffener debonding failure [4–8].

Out-of-plane joints are often co-cured with the skin during manufacturing to improve the integrity of the product and remove the assembly cost and added weight of fasteners. Moreover, composite materials are restrained by manufacturing constraints such as the minimum radius a ply can form. Subsequently, a deltoid shaped void is generated in the junction region of the skin, web and flanges. Such a feature is undesirable in a load-bearing structure and is usually filled with a filler material to eliminate the stress concentrations and ensure the geometrical stability of the joint.

The most commonly used filler is a bundle of unidirectional (UD) fibre, also known as a "noodle" when manufactured from a manually rolled ply. However, it is not only labour intensive to manufacture a noodle, but due to its orientation, weak transverse tensile strength and the loading conditions of out-of-plane joints, fillers can be the weakest link in the structural integrity of stiffened panels [9].

Search for stronger and more cost-effective fillers has been an important topic in the literature over recent years [10]. Braided and 3D woven fillers can be used to increase the strength of the joint and eliminate the need for rolling during manufacturing. In one example, the initial failure load of T-joints with braided fillers subjected to pull-off loading was increased by 36% compared to the conventional rolled specimens [11]. The main drawbacks of this solution are the restrictions of resin infusion processes and possible insufficient compaction of the filler during cure. Thermoplastic and foam fillers can be injection moulded, but this procedure needs the additional step of CNC machining of the filler to its final geometry [12,13]. However, the filler can be over-moulded on the laminate in a butt-joint configuration if the laminate is also made of thermoplastic matrix. Baran et al. developed an FEA model to analyse the cracking and debonding of a short fibre reinforced polyetheretherketone (PEKK) filler [14]. Through-the-thickness reinforcements such as stitching and pinning can greatly enhance the strength and damage tolerance of the joint, but the manufacturing time and cost are increased significantly [15,16]. Interleaving the joint with nonwoven veils can also increase its mechanical performance. Wang and Soutis [17] reported a 44% increase in ultimate tensile strength of a T-joint interleaved with polyester (PE) veils compared to a pristine one, but this method is also limited to resin infusion. A cost-effective manufacturing process is pultrusion, but this requires the in-situ curing of the whole stiffener section and therefore it cannot be used for manufacturing individual fillers for later assembly in a prepreg structure [18].

In this paper, the following eight novel concepts are introduced aimed at increasing the strength of fillers and out-of-plane joints or reducing their manufacturing time and cost:

- Filler surface interleaved with polyamide (PA) nonwoven mat (Fig. 1a)
- Filler surface interleaved with vertically aligned nanotubes (Fig. 1b)
- Filler surface and laminate interleaved with nonwoven nanofibre interleaves (Fig. 1c)
- 3D printed thermoplastic filler (Fig. 1d)
- Filler made of UD chips (Fig. 1e)
- Filler made of woven chips (Fig. 1f)
- Resin infused single braided filler (Fig. 1g)
- Resin infused multiple braided filler (Fig. 1h).

The new concepts are implemented in a T-joint and tested under tensile loading. The results are compared with a T-joint containing a manually rolled UD noodle (referred to as “baseline” in this paper).

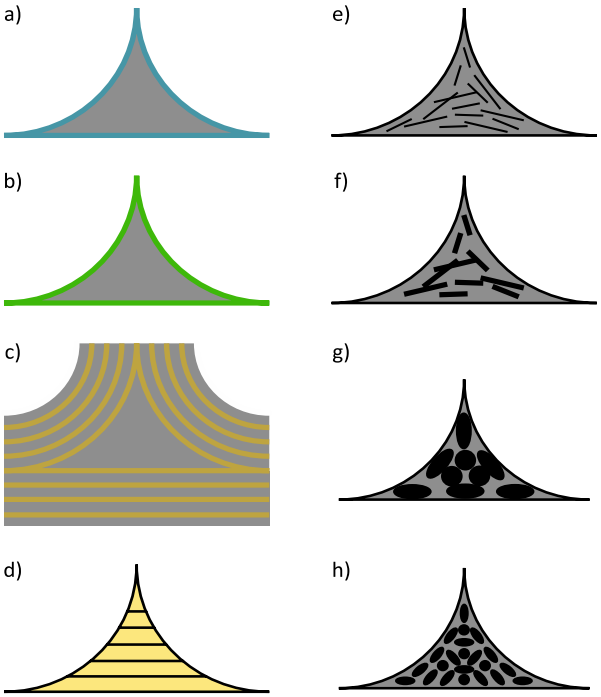

Fig. 1. Schematic representation of the proposed concepts: a) PA nonwoven interleaved b) Vertical nanotube interleaved c) Nonwoven nanofibre interleaved d) 3D printed e) Chopped UD f) Chopped woven g) Single braided h) Multiple braided

## 2. Manufacture of baseline joint and experimental setup

The manufacturing of the 6 baseline specimens is introduced in detail in [19] and is only described briefly in this work. The manufacturing of the 3 specimens used for each of the novel concepts are based on the same procedure and their distinct features are outlined in Section 3.

The geometry and the boundary conditions of the tensile test are shown in Fig. 2. Hexcel HexPly® AS4/8552 unidirectional prepreg [20] was used with a nominal cured ply thickness (CPT) of 0.196 mm. The stacking sequence of the overlaminate and skin were $[90/45/0/-45]_{2s}$ and $[90/45/0/-45]_{3s}$, respectively, where 0° is aligned in the Z direction. The plies are referred to as Ply 1 to Ply 16 in the overlaminate, with Ply 1 being adjacent to the filler (0°).

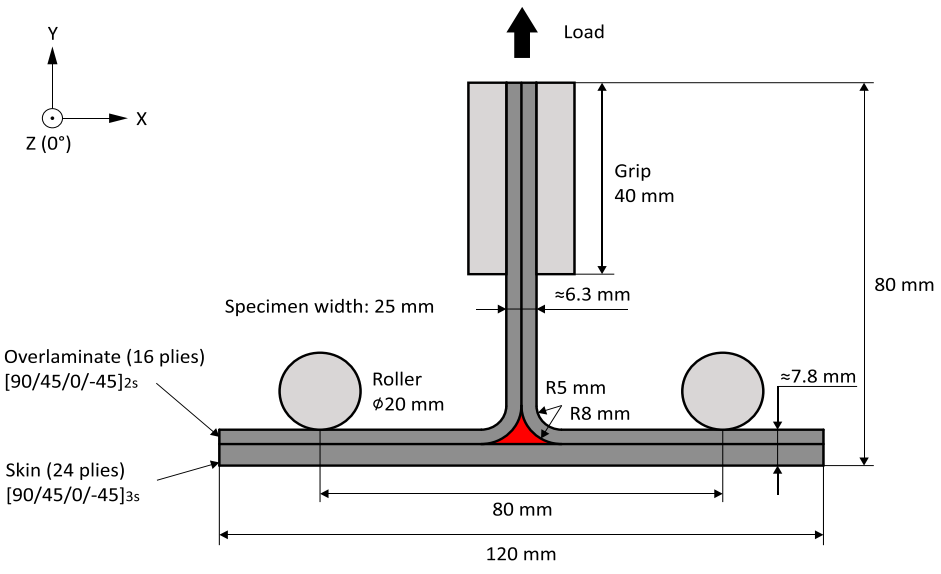


Fig. 2. Specimen geometry and test setup

The baseline filler was manufactured by manually rolling a ply having the same cured cross-sectional area as the theoretical deltoid shape. Then, it was placed in a noodle forming tool

(Fig. 3a), and the final geometry was achieved by a two-step procedure. First, heat was applied to increase formability while the filler was preformed with a caul plate and manual pressure, then the tool was closed and vacuum bagged to undergo debulking.

The steel tool used for curing consisted of two overlaminate tools, a caul plate for the skin and resin dams for sealing (Fig. 3b). The sublaminates were debulked after laying up every 4 plies. To ensure the consistent temperature distribution during curing, the lowest allowable heat up and cool down rates were chosen according to the manufacturer's datasheet [20]: heat at 1 °C/min up to 110 °C, hold for 1 hour, heat at 1 °C/min up to 180 °C, hold for 2 hours, cool at 2 °C/min to room temperature.

After curing, the individual samples were cut and surfaces were ground to P2500 quality.

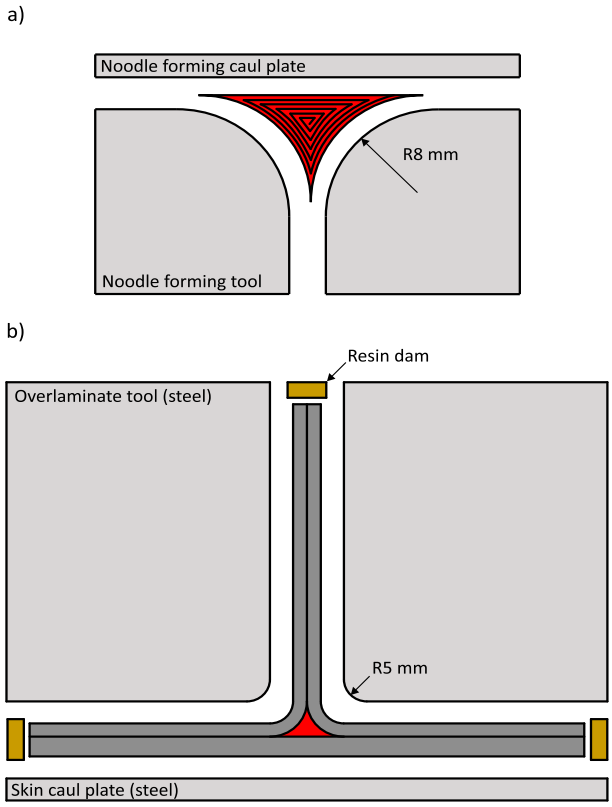


Fig. 3. a) Noodle forming tool b) T-joint tool

The specimens were heated to 120 °C for 2 hours before testing to eliminate the moisture content accumulated after manufacturing. The tests were carried out at 2 mm/min crosshead displacement rate and at room temperature with an Instron 3369 machine. Deformation in the vicinity of the fillers was recorded with Phantom VEO 410L high-speed cameras and displacement was taken as the crosshead displacement of the Instron machine.

## 3. Manufacture of the alternative concepts

### 3.1. Interleaved joints

Delamination of the interface between the filler and the adjacent ply, or within the laminate in an out-of-plane joint is one of the most common failure mechanisms of stiffeners [10]. A common method to increase the delamination strength is to interleave the plies with a toughening material such as nonwoven mats, particulates, thermoplastic films or adhesive films [21]. In this work, three concepts are investigated: use of a polyamide (PA) nonwoven mat, a layer of vertical nanotubes, and a nonwoven nanofibre mat combined with a conventional rolled noodle.

Due to their easy handling, nonwoven mats are often used with non-crimped fabric (NCF) laminates and resin infusion. However, they are not intended to be used with prepregs due to the fixed resin content of the latter. To evaluate their behaviour embedded in a prepreg laminate, double cantilever beam (DCB) and end notched flexure (ENF) tests [22,23] were carried out on several nonwoven mats to characterise their mode I and II fracture toughnesses [24]. The results indicated the most significant fracture toughness improvement of the Cerex PBN-II® 30100 PA mat (Cerex Advanced Fabrics Inc., referred to as “PA” in this paper) with 0.2 mm dry thickness and 34 gsm weight [25], which was chosen for this study accordingly. Compared to pristine AS4/8552 specimens, the PA mat provided over 250% improvement in mode I, and over 80% improvement in mode II fracture toughness, respectively. As these

values refer to the energy release rate at crack initiation, this can indicate the improved interfacial strength of a PA interleaved laminate.

The first concept was produced by placing one layer of the PA nonwoven mat between the filler and Ply 1 in the radius, in the midplane of the web and flanges and under the filler (Fig. 4a) during the assembly of the T-joint.

The second concept was based on the N12 NanoStitch® layer. This can reinforce the interface between two adjacent plies with a vertical nanotube forest and increase the toughness and damage tolerance of the laminate [26]. The 0° plies in the midplanes of the T-joint (Ply 1 in the overlaminate and top ply of the skin) were treated with N12 NanoStitch® nanotubes and the joint was manufactured as mentioned above (Fig. 4a).

The third concept involved the interleaving of all interfaces within the laminate in the vicinity of the radius and skin around the filler with a 4.5 gsm Xantu.Layr® (Revolution Fibres Ltd., [27]) nonwoven nanofibre mat (Fig. 4b). Unlike the PA mat, this interleaf has virtually zero thickness and is developed to be used with prepreg materials, and therefore did not produce a noticeable change in the radius thickness of laminate around the filler.

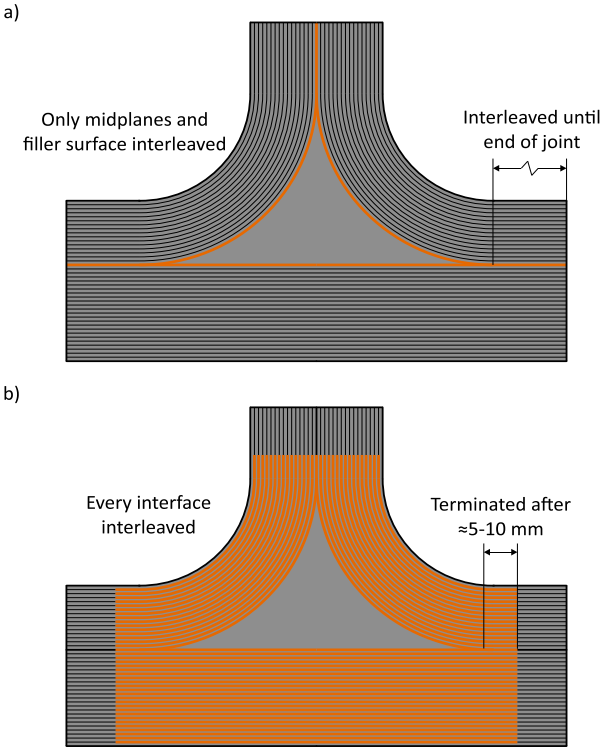


Fig. 4. Location of interleaves in the T-joint: a) PA and NanoStitch® b) Xantu.Layr®

### 3.2. 3D printed thermoplastic filler

Due to the recent development of high-performance substances and manufacturing processes, thermoplastic composites are becoming a viable choice of material for primary aerospace structures. However, they are generally manufactured as individual components, and not co-cured with a thermoset laminate. The concept presented in this work is a 3D printed thermoplastic filler, co-cured with the epoxy matrix based laminate of the T-joint. This concept combines the high production rate using prepreg materials, the low labour requirement of additive manufacturing, and the comparable or marginally higher strength of thermoplastic materials compared to the transverse tensile strength of thermoset resin based composites.

In order to co-cure a thermoplastic filler with the thermoset laminate and implement it in an out-of-plane joint, the material needs to meet three requirements. First, it must have higher melting temperature than the cure temperature of the thermoset resin in the laminate (which

is 180 °C for Hexcel 8552 used in this work), otherwise the geometry could not be retained during the curing of the joint.

Second, the thermoplastic material must be compatible with the thermoset resin. To quantitatively measure this, bimaterial fracture toughness tests should be carried out with the used thermoset resin and representatively manufactured thermoplastic materials. However, such experimental characterisation was out-of-scope for this work.

Third, the thermoplastic material should have comparable or higher yield strength than the transverse tensile strength of the thermoset composite material, as the latter is the driving factor for influencing the strength of a conventional UD composite noodle [10]. Note that the strength of a 3D printed structure differs from the strength of a component which has been injection moulded from the same material [28].

There are many high temperature, high strength thermoplastic materials used in aerospace applications. However, to the authors' best knowledge, only polyetherimide (PEI) has been demonstrated in the literature to meet the second criterion, i.e. to be compatible with epoxy thermoset resins [12,29]. Therefore, ULTEM™ 1010 polyetherimide was chosen as filler material in this work. According to the manufacturer's datasheet [30], the longitudinal tensile strength is 56 MPa. This and the transverse tensile strength were evaluated by the authors with 5 repeats of dog bone tensile tests based on [31]. The 3D printed coupons were printed in longitudinal and transverse directions with patterns printed according to [28]. Nominal voxel size was 0.1 mm and they were manufactured with an in-house built fused deposition modelling (FDM) printer. Extruder temperature (385 °C), bed temperature (140 °C) and print speed (20 mm/s) were set up according to the manufacturer's recommendations [30]. Then, the specimens were annealed to eliminate the thermal stresses accumulated during printing (kept at 150 °C for 1 hour, kept at 205 °C for 1 hour, kept at 150 °C for 30 minutes, cooled

down to room temperature). The measured longitudinal and transverse tensile strength values were found to be 64 MPa and 55 MPa, respectively.

The 3D printed filler had the same dimensions as described in Section 2 and was printed with the same parameters as the tensile test specimens. The printing direction was chosen along axis Y. This eliminated the need for any support structure and the filler radius could be sufficiently reproduced with the 0.1 mm voxel size. After fabrication and annealing, the 3D printed filler was deburred, assembled and cured within the T-joint assembly according, to Section 2.1.

### 3.3. Chopped fillers

One way to reduce the manufacturing cost of fillers is to use wastage material left behind from ply cutting and replace the manual noodle forming step with an automated process. The following solution is a filler made of randomly oriented UD and woven prepreg chips and injected into a forming tool. However, as this is a proof of concept, the latter step was replaced by manual cutting and assembly in this work.

Hexcel HexPly® AS4/8552 material was used for the UD chips, whereas Hexcel HexForce™ AGP280-5H [32] was used for the woven chips. The latter consists of the same AS4 fibres [33] and 8552 resin [20] but has a 5 harness satin woven structure and nominal ply thickness of 0.29 mm. In theory, the chip size should be as small as possible so that the mechanical behaviour of the filler approaches isotropic; but large enough so that the fibre length is larger than the critical fibre length, which is 0.18 mm (calculated using fibre diameter from [33]) for AS4/8552 with 3K tow size. Based on preliminary trials, a 5x5 mm chip size was chosen for both concepts, as smaller pieces of UD prepreg fell apart during handling. However, the authors note that the woven prepreg can be cut into smaller pieces due to its more stable woven structure. After cutting the same volume of prepreg material as used in the rolled

noodle, the chips were placed into the noodle forming tool (Fig. 3a), debulked, and finally assembled within the T-joint (Fig. 5). After curing and cutting, the specimens were scanned with a Nikon XT H 225 ST CT scanner (Perkin Elmer 1620 16-bit flat panel detector, voltage: 157 kV, current: 157 µA, exposure time: 500 ms, average number of projections: 2930, voxel size: 0.02 mm) and scans examined with Avizo 9 software to measure the porosity.

Fig. 5. Underside view of the chopped UD filler before the assembly of the overlaminates and the skin

**3.4. Braided fillers**

Due to their freedom in achievable geometry and increased out-of-plane strength, utilisation of braided components is one of the most advantageous features of structures manufactured with resin infusion. The proposed concept combines commercially available braided fillers with the pre-impregnated laminate of the T-joint. Unlike conventional prepreg noodles, which require labour intensive in-situ rolling and forming during the manufacturing of the stiffeners, the dry braids can be infused and stored in a freezer, independently from the assembly, greatly reducing the manufacturing time of the structure.

Two different fillers were manufactured from Eurocarbon's commercially available product line [34]: one made of a single braid having 28.3 $mm^2$ cross-sectional area (referred to as "single braided" in this paper) and one made of eight smaller braids each having 3.6 $mm^2$ cross-sectional area (28.8 $mm^2$ in total; referred to as "multiple braided" in this paper). These correlate with the theoretical 27.5 $mm^2$ cured cross-sectional area of the rolled noodle. The latter method was implemented to reduce the resin rich zones and poor compaction of the single braid noodle reported in the literature [35]. Hexcel HexFlow® RTM 6 thermoset resin [36] was used for the infusion, which has the same 180 °C cure temperature as 8552. After removal from the noodle forming tool, the fillers were assembled (Fig. 6) and cured within the joint according to Section 2. Porosity measurement with CT scanning was carried out as described in the previous section.

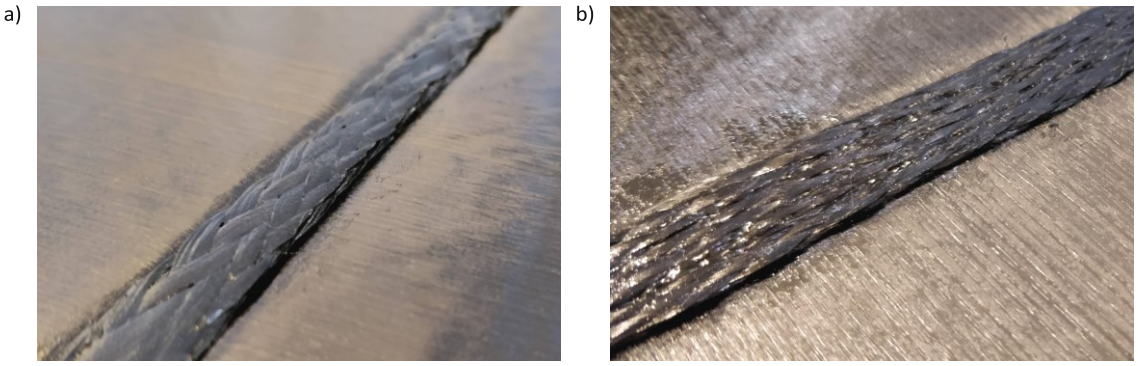


Fig. 6. Underside view of the braided fillers before the assembly of the overlaminates and the skin: a) single braided b) multiple braided

## 4. Results and discussion

### 4.1. Manufactured specimens

Micrographs of the typical cross-sections of the manufactured baseline and proposed fillers can be seen in Fig. 7-8. In the baseline joint (Fig. 7), the skin is flat under the filler and its geometry is virtually identical to the theoretical one. The measured 0.181 mm ply thickness of

the radius is 8% lower than the nominal 0.196 mm of AS4/8552. For detailed discussion on the quality of the baseline filler, the authors refer to [19].

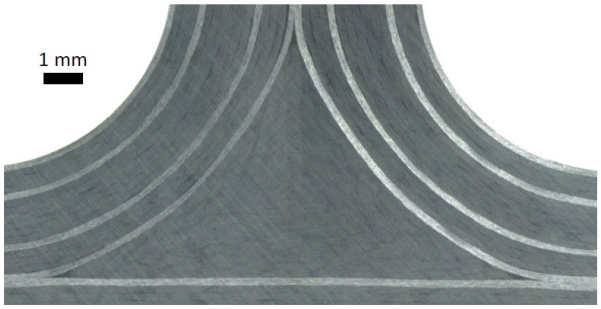


Fig. 7. Micrograph of the manufactured baseline filler

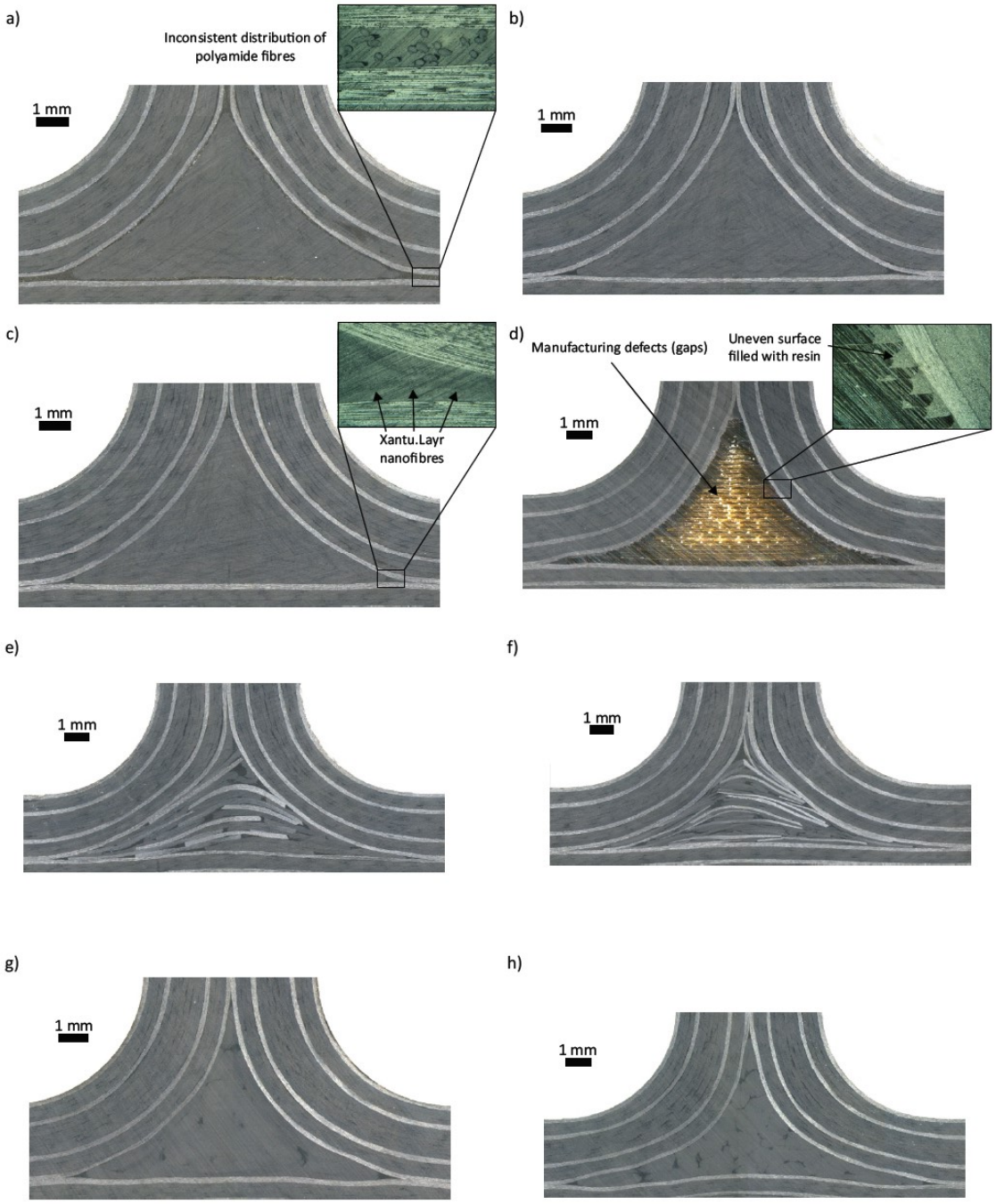


Fig. 8. Micrographs of the manufactured fillers: a) PA nonwoven interleaved b) NanoStitch® vertical nanotube interleaved c) Xantu.Layr® nonwoven nanofibre interleaved d) 3D printed e) chopped UD f) chopped woven g) single braided h) multiple braided

The PA nonwoven interleaved, NanoStitch® vertical nanotube interleaved and Xantu.Layr® nonwoven nanofibre interleaved specimens can be seen in Fig. 8a-c. The PA veil significantly

increased the thickness of the interface between the filler and Ply 1, but its thickness is inconsistent in some locations due to its nonwoven nature, consisting of randomly oriented fibres. At a higher magnification, the inconsistency of the fibre volume ratio can also be seen. The NanoStitch® vertical nanotubes are not visible even at 50x magnification with the optical microscope. The Xantu.Layr® veils resulted in only 3 μm thickening of the interface based on measurements from micrographs, but this value might fall within the variability of the prepreg CPT in the radius [19]. The outline of the veils is visible in the right edge of the filler highlighted in Fig. 8c.

Only after cutting the specimens with 3D printed filler (Fig. 8d) was it revealed that in certain cross-sections along the length of the filler, the printer incorrectly reproduced the layers and gaps appeared inside the middle of the deltoid (bright areas in Fig. 8d as a result of different light reflection). It is assumed to be in connection with the code generated for printing, the capabilities of the 3D printer used and the printing parameters set up. Achieving higher quality should be possible with an industrial grade printer and fine-tuning of the printing parameters. Nevertheless, the geometry of the filler surface is satisfactory as the thermoset resin filled the uneven surface caused by the discrete steps of the printed layers, ensuring a smooth transition of Ply 1 of the overlaminate from the skin to the web.

The chopped UD and woven fillers can be seen in Fig. 8e-f. The average width of the fillers (15.7 mm and 15.6 mm for UD and woven, respectively) were 17% higher compared to the baseline case (13.4 mm) and varied across the cut specimens, which is caused by the random orientation and location of chips across the length of the filler (Fig. 5). The width was measured based on micrographs (e.g. Fig. 8) and is defined as the distance between the bottom edges of the filler. The width variability can be reduced with smaller chip size and an automated procedure using a closed noodle forming tool. Subsequently to the wider and

higher filler, as the filler volume was fixed, the ply thickness was increased in the radius and the skin under the filler became non-flat. During manufacturing, the filler forming tool was filled up with chips being generally parallel to the skin or rotated along the Z-axis. This resulted in a marginally increased resin-rich zone near the top edge of the filler, and lack of chips being parallel to the X-Y-plane. The CT scan revealed <0.1% porosity content in both fillers, but this is within the boundaries of the maximum of 2.5% allowable void content in aircraft components [37]. The largest void had 0.17 mm and it is shown in Fig. 9. Note that the black areas in the fillers in Fig. 8g-h) are resin rich pockets and not porous zones.

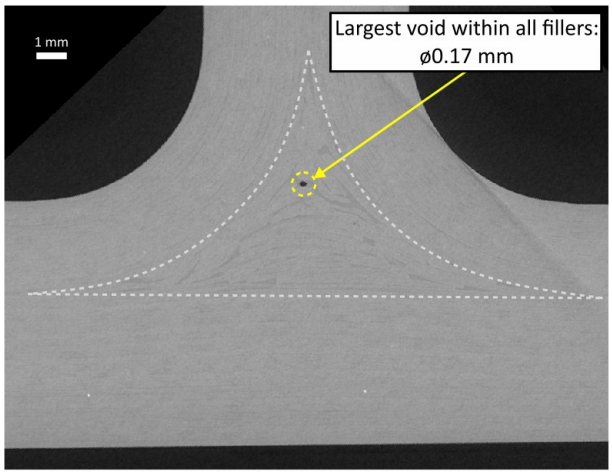


Fig. 9. CT scan image of a chopped filler with the largest void shown

The single and multiple braided fillers are shown in Fig. 8g-h. Similarly to the chopped concepts, the width of the multiple braided fillers increased (15.7 mm, 17% increase compared to baseline), as well as the ply thickness in the radius. Contrarily, the single braided filler had superior compaction and retained its geometry (same width as the baseline) with significantly less resin-rich areas within it. The reason for this is that the multiple braided fillers contain 8 individual braids which are less resistant to the applied pressure and resin movement in the joint during curing, whereas the single braided fillers have higher integrity and can withstand

the acting forces on them more sufficiently. Based on the CT scan analysis, the braided fillers did not contain any voids.

### 4.2. Test results and failure mechanisms

Due to the large number of specimens, only one typical load-displacement curve of each concept is presented (Fig. 10), and the complete list of initial failure loads can be found in Table 1. Micrographs of the failed specimens can be seen in Fig. 11-12.

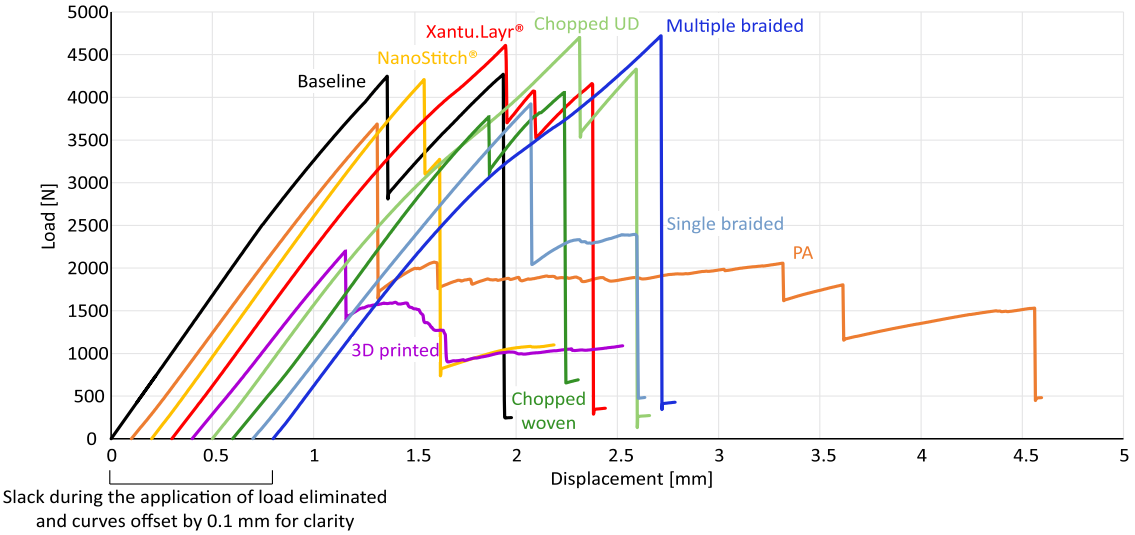


Fig. 10. Typical load-displacement curves of the experimental tests

Table 1. Test results. Load-displacement curves of the specimens in bold are shown in Fig. 10.

| Concept | ID | Initial failure load [N] | Avg. (SD) [N] | Diff. [%] |
|---|---|---|---|---|
| **Baseline** | A1 | 3907 | 4366 (330) | - |
| | A2 | 4818 | | |
| | A3 | 4147 | | |
| | **A4** | 4235 | | |
| | A5 | 4560 | | |
| | A6 | 4527 | | |
| **PA** | IA1 | 3257 | 3257 (440) | -25% |
| | IA2 | 2809 | | |
| | **IA3** | 3687 | | |
| **NanoStitch®** | **N1** | 4208 | 4384 (223) | 0% |
| | N2 | 4308 | | |

| | | | | |
|---|---|---|---|---|
| | N3 | 4635 | | |
| **Xantu.Layr®** | **X1** | 4601 | 4627 (136) | +6% |
| | X2 | 4506 | | |
| | X3 | 4775 | | |
| **3D printed** | P1 | 2603 | 2510 (278) | -43% |
| | **P2** | 2197 | | |
| | P3 | 2730 | | |
| **Chopped UD** | CU1 | 4507 | 4589 (106) | +5% |
| | **CU2** | 4709 | | |
| | CU3 | 4552 | | |
| **Chopped woven** | CW1 | 4107 | 4112 (343) | -6% |
| | CW2 | 4457 | | |
| | **CW3** | 3771 | | |
| **Single braided** | **VS1** | 3924 | 3401 (1118) | -22% |
| | VS2 | 2052 | | |
| | VS3 | 4226 | | |
| **Multiple braided** | **VM1** | 4723 | 2510 (422) | +2% |
| | VM2 | 3984 | | |
| | VM3 | 4705 | | |

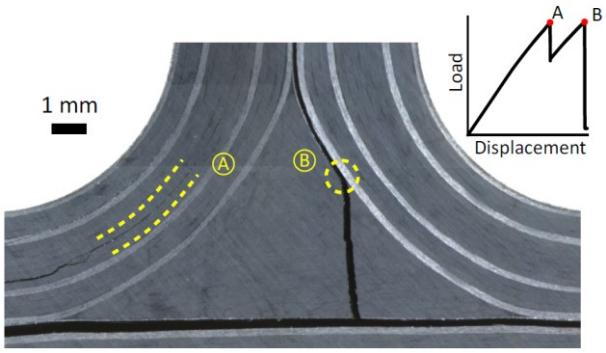


Fig. 11. Micrograph of the failed baseline filler. For interpretation of the load-displacement curve see Fig. 10

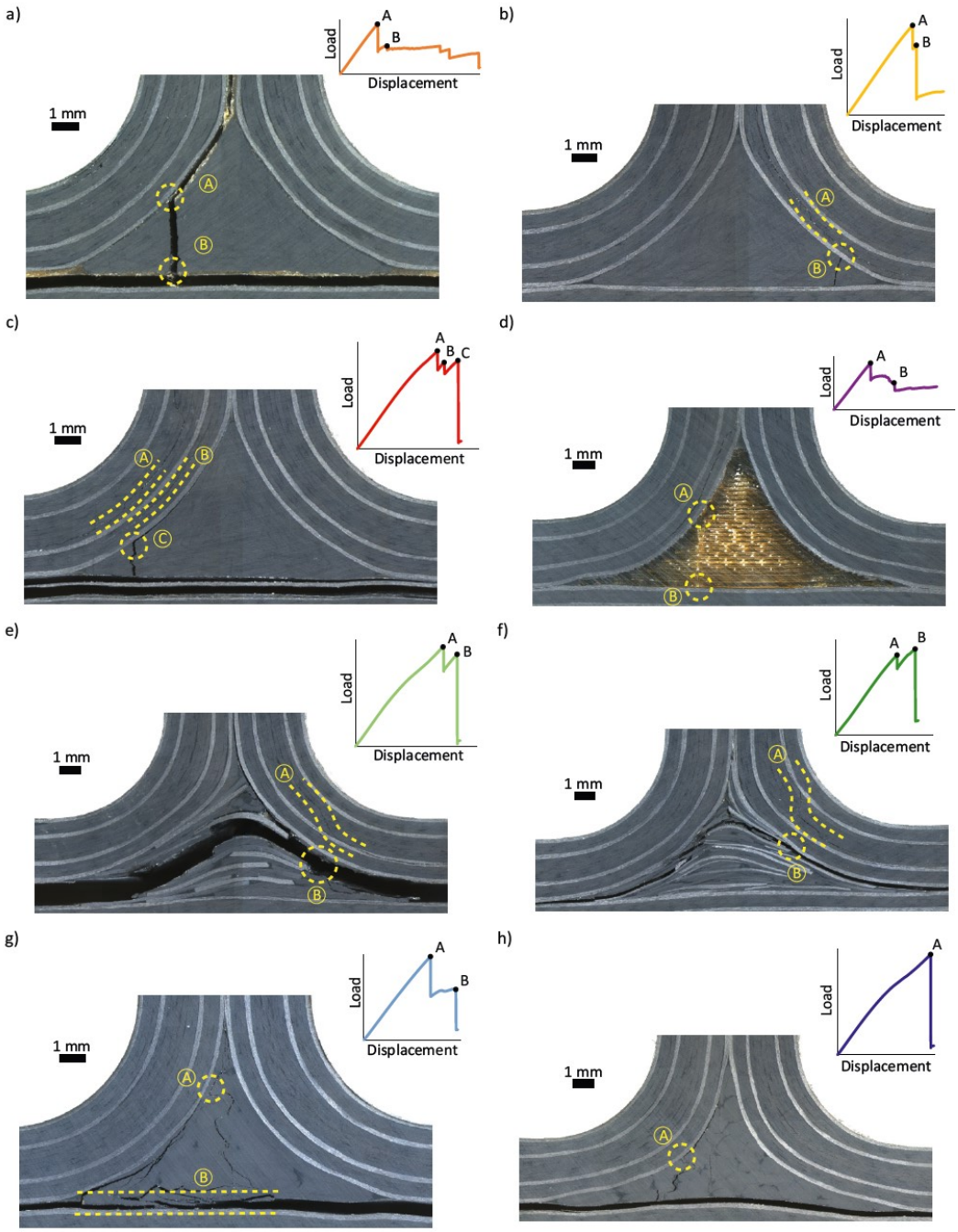


Fig. 12. Micrographs of the failed fillers: a) PA nonwoven interleaved b) NanoStitch® vertical nanotube interleaved c) Xantu.Layr® nonwoven nanofibre interleaved d) 3D printed e) chopped UD f) chopped woven g) single braided h) multiple braided. For interpretation of the load-displacement curves see Fig. 10

Baseline specimens A1-A4 and A6 had similar failure initiation. After the linear load-up stage a crack initiated in the radius, causing the first drop in the load-displacement curve (Fig. 11 point A). This was followed by either one or more further cracks in the laminate or the crack of the filler (Fig. 11 point B). The filler crack propagated from the surface of the filler down to the skin and triggered delamination along the surface of the filler and under the filler. The laminate of specimen A5 remained intact and its filler cracked first.

The polyamide interleaved joints all had a filler crack as the first failure event (Fig. 12a, point A) at average of 25% lower load than the baseline joints. The reason for this knockdown is probably the insufficient infusion of the dry mat by the resin during curing and the subsequent porosity near groups of entangled PA fibres. With consistent fibre distribution in the mat and lower interface thickness to reduce the amount of resin needed from the prepreg plies to wet the dry veil, it is possible that the drop in interface strength could be mitigated. Similarly to the baseline joints, the crack propagated down to the skin and caused delamination on the filler surface up to the web, but could not trigger delamination immediately under the filler and the joint withstood further loading. Finally, the skin gave in (Fig. 12a, point B) and started delaminating. However, the improved damage tolerance can be seen in Fig. 10, as the joint carried about 2000 N load during skin delamination and absorbed a relatively higher amount of energy, whereas most other joints could only take about 500 N following initial failure. There were no independent displacement measurements utilised other than the cross-head displacement of the Instron machine, which suffers from compliance error. Thus, the absorbed energy should not be quantified and the comparison is merely based on visual observation of the curves in Fig. 10.

The NanoStitch® interleaved joints behaved similar to the baseline joints both in terms of failure mechanisms (Fig. 12b, point A and B referring to radius laminate and filler crack,

respectively) and average initial failure load (<1% difference). Specimens N2 and N3 did not achieve a second peak after initial failure. Because the initial failure did not occur in the filler-laminate surface, the NanoStitch® layer could not alter the failure behaviour here. However, the nanotube forest under the filler and across the skin-overlaminate interface did not alter the failure mechanism during the delamination of the skin either. To balance the more complex manufacturing procedure, a significant improvement would be needed in performance to consider this concept as a viable solution. It is also possible that NanoStitch® nanotubes work better with toughened resin (such as TC350-1 in [26]), but are not able to improve the properties of the 8552 resin used in this work.

The Xantu.Layr® interleaved specimens reached the highest average initial failure load of all proposed concepts (6% higher than baseline, which is significant, based on one-sided T-test analysis). The failure mechanisms were similar to the ones occurring in the baseline joints as the overlaminate cracked first in case of X1 and X2 specimens (Fig. 12c, point A). However, further cracks occurred in the laminate (Fig. 12c, point B), followed by the final filler crack (Fig. 12c, point C) and sudden drop in load. The X3 specimen failed with the filler crack as the first sign of damage initiation. The increased interlaminar strength of the laminate is reflected in the increased overall joint strength. Therefore, this solution can be applied in highly loaded regions of components where the strength improvement outweighs the marginal increase in manufacturing complexity.

As mentioned in the previous section, the 3D printed fillers suffered from manufacturing defects. This was reflected in the results as all three joints failed initially with cracking of the filler (Fig. 12d, point A) at 57% lower average initial failure load compared to the baseline case. In specimen P1, the laminate remained intact, whereas in P2 and P3 specimens it was immediately followed delaminations in the overlaminate. However, because of the high

fracture toughness of PEI material, the filler crack could not propagate and reach the skin immediately and the joint absorbed more energy before the filler-skin interface failed (Fig. 12d, point B). Despite the lower strength of the joints, the interface of the 3D printed filler and Ply 1 of the overlaminate did not fail in any cases. This proves that the cohesion between the thermoplastic PEI and the thermoset 8552 materials is sufficient for structural applications.

Chopped UD and woven joints initially failed with radius delaminations at 4589 N and 4112 N average loads, respectively (Fig. 12e-f, points A). These values correspond to +5% and -6% difference compared to the baseline configuration. However, the failure of the chopped fillers (Fig. 12e-f, points B) differed from the failure of the rolled noodles. In the latter case, the noodle fails because its low transverse tensile strength cannot withstand the loads acting on it from the opening mechanism of the radius. The crack then propagates without any significant resistance down to the skin. In the case of the chopped fillers, most of the inside surfaces (filler side) of Ply 1 in the overlaminate are covered with chips following the curvature of the ply. This provides protection from the opening mechanism of the radius, unless the fibre orientation of the chip is the same as of a noodle, which is unlikely. Therefore, the crack can only initiate at the end of a chip (“chip drop”) where the resin is accumulated such as the one highlighted in Fig. 12f. Then the crack propagates along the surfaces of the chips until reaching the other side of the filler and delaminating the skin from the flanges. In this manner, the orientation and location of the chips define the crack initiation location and the way how the crack propagates within the filler. This could be used to change the failure behaviour of the filler, but the level of control over the chip orientation and location is limited in practice. Subject to the achievable level of automated manufacturing procedure, chopped fillers are feasible solutions to replace the currently utilised rolled UD noodles.

In all six cases of the single and multiple braided specimens, the joints failed in the filler (Fig. 12g-h, points A) and the overlaminate remained undamaged. The average initial failure loads were 3401 N and 4471 N respectively, resulting in -22% and +2% difference compared to the baseline joints. It is notable that VS2 specimen failed at 2052 N, which is the lowest initial failure load of the 30 specimens tested, and VM2 failed at 3984 N, which also significantly differs from the average value. These can be accounted for the variability of cross section across the length of the noodle, leading to alteration of fibre-rich and resin-rich zones on the filler surface in different cross sections. Due to the non-0° orientation of the braided fibres, the crack could not propagate downwards directly and had to change its direction several times while developing several smaller cracks. In some cases, the skin delamination was delayed by almost horizontal cracking of the bottom of the filler (Fig. 12g, until point B). The main difference between the single and multiple braided specimens was the location of the crack initiation in the filler. In the first case, it started higher and closer to the top edge of the deltoid, and in the latter case, it started at a similar location as in the case of the rolled noodle. Most probably, this is because the multiple braided fillers have fibres oriented closer to 0° than the fibres in the single braided filler. As the interface of the filler and Ply 1 did not fail, it is demonstrated that curing together an infusion resin (RTM6) and prepreg resin (8552) can provide sufficient strength in the structure. With the reduced cost of the proposed manufacturing procedure, resin infused braided fillers are a highly favourable choice to replace conventional rolled noodles.

## 5. Conclusions

Eight novel filler concepts were introduced to increase the strength of composite out-of-plane joints or decrease the manufacturing cost and time of their filler. The new solutions were

manufactured as part of a T-joint, tested under tensile (pull-off) loading and compared with the conventional rolled UD filler ("baseline") material.

The results demonstrated that polyamide nonwoven interleafs can increase the damage tolerance of the structure even if manufactured as part of a prepreg laminate, but they reduce the strength of the interface at the same time. NanoStitch® vertical nanotubes did not alter the behaviour of the joint in this specific application. Xantu.Layr® nonwoven nanofibre veils increased the initial failure load of the joints by 6% and can be used as a viable solution in highly loaded components.

3D printed fillers suffered from manufacturing defects and subsequent drop in strength, but showed that the cohesion between the thermoplastic and thermoset resins is sufficiently strong and the weakest link in hybrid components is not the bimaterial interface. With the application of high strength, high temperature and epoxy compatible thermoplastic resins, 3D printed fillers with improved manufacturing quality and extruded or injection moulded fillers can replace the labour intensive rolled noodles.

Fillers manufactured from chopped unidirectional and woven chips yielded essentially the same strength as the baseline filler (+5% and -6% in comparison). With further development in the manufacturing procedure, such as using waste prepreg material and automated cutting and injection moulding of the chips, this concept can become a high production rate alternative of currently used methods.

Finally, braided fillers consisting of resin infused single and multiple braids cured together with the prepreg laminate of the T-joint were manufactured and tested. While the single braided concept failed at 22% lower load than the baseline, the multiple braided filler was 2% stronger. Moreover, all specimens failed without delaminating the interface of the filler and the laminate, which demonstrates that the different infusion and prepreg resins formed a strong

bond. This means that resin infused fillers can not only match the strength of the unidirectional rolled fillers, but also significantly reduce the manufacturing cost and time of out-of-plane joints.

The new solutions demonstrated in this paper can be used to increase the strength, reduce the cost and reduce the manufacturing time of composite out-of-plane joints. In addition, the radical concept of hybridising thermoplastic and thermoset resins, and different type of thermoset resins within the same structure and in the same cure cycle opens up a wide range of new applications involving the combination of thermoplastic, infused braided, 3D woven and thermoset prepreg materials.

**Acknowledgement**

Zsombor Sápi would like to thank GKN Aerospace Ltd. for sponsoring the project. Richard Butler holds a Royal Academy of Engineering – GKN Aerospace Research Chair. The authors are grateful for Matthew Shorter (GKN Aerospace) for the help provided with the resin infusion of braided fillers, and Dr Robert J. A. Allen† (University of Bath, deceased on 4th September 2017) and Dr Simon R. G. Bates (University of Bristol) for the help provided with the manufacturing of 3D printed specimens. The authors would like to thank Cerex Advanced Fabrics Inc., N12 Technologies Inc., Revolution Fibres Ltd. and Eurocarbon B. V. for providing materials.

**References**

[1] Herencia JE, Weaver PM, Friswell MI. Optimization of long anisotropic laminated fiber composite panels with T-shaped stiffeners. AIAA Journal 2007;45:2497–509. doi:10.2514/1.26321.

[2] Kong CW, Lee IC, Kim CG, Hong CS. Postbuckling and failure of stiffened composite panels under axial compression. Composite Structures 1998;42:13–21.

doi:10.1016/S0263-8223(98)00044-0.

[3] Talezadehlari A, Rahimi GH. Optimization for buckling loads of grid stiffened composite panels. Composite Structures 2016;135:409–10. doi:10.1016/j.compstruct.2015.09.006.

[4] Orifici AC, Shah S a., Herszberg I, Kotler A, Weller T. Failure analysis in postbuckled composite T-sections. Composite Structures 2008;86:146–53. doi:10.1016/j.compstruct.2008.03.022.

[5] Shishesaz M, Hosseini M. Effects of joint geometry and material on stress distribution, strength and failure of bonded composite joints: an overview. The Journal of Adhesion 2018. doi:10.1080/00218464.2018.1554483.

[6] Riccio A, Raimondo A, Di Felice G, Scaramuzzino F. A numerical procedure for the simulation of skin-stringer debonding growth in stiffened composite panels. Aerospace Science and Technology 2014;39:307–14. doi:10.1016/j.ast.2014.10.003.

[7] Camanho PP, Davila CG, Pinho SS. Fracture analysis of composite co-cured structural joints using decohesion elements. Fatigue and Fracture of Engineering Materials and Structures 2004;27:745–57. doi:10.1111/j.1460-2695.2004.00695.x.

[8] Psarras S, Pinho ST, Falzon BG. Damage-tolerant design of stiffener run-outs : A finite element approach. In: Ebrahimi F, editor. Finite Element Analysis - New trends and developments, InTech; 2012, p. 277–300. doi:10.5772/50377.

[9] Hélénon F, Wisnom MR, Hallett SR, Trask RS. Numerical investigation into failure of laminated composite T-piece specimens under tensile loading. Composites Part A: Applied Science and Manufacturing 2012;43:1017–27. doi:10.1016/j.compositesa.2012.02.010.

[10] Sápi Z, Butler R, Rhead A. Filler materials in composite out-of-plane joints – A review.

Composite Structures 2019;207:787–800. doi:10.1016/j.compstruct.2018.09.102.

[11] Li X, Liu Z, Hu L, Wang Y, Lei B, Huang X. Numerical investigation of T-joints with 3D four directional braided composite fillers under tensile loading. Applied Composite Materials 2016;24:171. doi:10.1007/s10443-016-9520-5.

[12] Heimbs S, Jürgens M, Breu C, Ganzenmüller G, Wolfrum J. Investigation and Improvement of Composite T-Joints with Metallic Arrow-Pin Reinforcement. In: Cloud GL, Patterson E, Backman D, editors. Joining Technologies for Composites and Dissimilar Materials, Volume 10: Proceedings of the 2016 Annual Conference on Experimental and Applied Mechanics, Springer International Publishing; 2017, p. 33–40. doi:10.1007/978-3-319-42426-2_4.

[13] Cui H. Delamination and debonding failure of laminated composite T-joints. PhD thesis. Delft University of Technology, 2014. doi:10.4233/uuid:fcf6a51a-1abd-4751-8ae5-338dbb23bce2.

[14] Baran I, Warnet LL, Akkerman R. Assessment of failure and cohesive zone length in co-consolidated hybrid C/PEKK butt joint. Engineering Structures 2018;168:420–30. doi:10.1016/j.engstruct.2018.04.089.

[15] Koh TM, Isa MD, Feih S, Mouritz AP. Experimental assessment of the damage tolerance of z-pinned T-stiffened composite panels. Composites Part B: Engineering 2013;44:620–7. doi:10.1016/j.compositesb.2012.02.017.

[16] Greenhalgh E, Lewis A, Bowen R, Grassi M. Evaluation of toughening concepts at structural features in CFRP-Part I: Stiffener pull-off. Composites Part A: Applied Science and Manufacturing 2006;37:1521–35. doi:10.1016/j.compositesa.2005.11.009.

[17] Wang Y, Soutis C. Fatigue behaviour of composite T-joints in wind turbine blade

applications. Applied Composite Materials 2016;24:461. doi:10.1007/s10443-016-9537-9.

[18] Schultz MR, Rose CA, Guzman JC, McCarville D, Hilburger MW. An experimental study of the compression response of fluted-core composite panels with joints. Composites Part B 2014;61:229–237. doi:10.1016/j.compositesb.2013.12.029.

[19] Sápi Z, Butler R, Rhead A. High fidelity analysis to predict failure in T-joints. Composite Structures 2019;225:111143. doi:10.1016/j.compstruct.2019.111143.

[20] Hexcel Composites. HexPly 8552 product data sheet, publication FTA 072e; 2013.

[21] Nash NH, Young TM, McGrail PT, Stanley WF. Inclusion of a thermoplastic phase to improve impact and post-impact performances of carbon fibre reinforced thermosetting composites - A review. Materials and Design 2015;85:582–97. doi:10.1016/j.matdes.2015.07.001.

[22] American Society for Testing and Materials. ASTM D5528 − 13: Standard test method for mode I interlaminar fracture toughness of unidirectional fiber-reinforced polymer matrix composites 2013.

[23] American Society for Testing and Materials. ASTM D7905/D7905M − 14: Standard test method for determination of the mode II interlaminar fracture toughness of unidirectional fiber-reinforced polymer matrix composites 2014.

[24] Sápi Z. Design, Analysis and Testing of Composite T-joints. PhD thesis. University of Bath, 2019.

[25] Cerex Advanced Fabrics. Cerex PBN-II 30100 product data sheet 2012.

[26] Conway H, Chebot D, Gouldstone C, Williams R. Fatigue response of carbon fiber epoxy

laminates with vertically-aligned carbon nanotube interfacial reinforcement. SAMPE Baltimore, 2015.

[27] Revolution Fibres. Xantu.Layr product brochure v5.4 2018.

[28] Torrado AR, Roberson DA. Failure analysis and anisotropy evaluation of 3D-printed tensile test specimens of different geometries and print raster patterns. Journal of Failure Analysis and Prevention 2016;16:154–64. doi:10.1007/s11668-016-0067-4.

[29] Villegas IF, van Moorleghem R. Ultrasonic welding of carbon/epoxy and carbon/PEEK composites through a PEI thermoplastic coupling layer. Composites Part A: Applied Science and Manufacturing 2018;109:75–83. doi:10.1016/j.compositesa.2018.02.022.

[30] 3DXTech. ULTEM 1010 3D printing filament technical data sheet v3.0 2018.

[31] American Society for Testing and Materials. ASTM D638 − 14: Standard test method for tensile properties of plastics 2014.

[32] Hexcel Composites. HexForce AGP280-5H product data sheet 2018.

[33] Hexcel Composites. Hexcel HexTow AS4 product data sheet, publication CTA 311 FB18 2018.

[34] Eurocarbon. Braided Aero Filler product data sheet 2018.

[35] Heimbs S, Mierzwa A, Duwensee T, Breu C, Nogueira AC, May M, et al. Investigation of static and dynamic failure behaviour of composite T-joints. 4th ECCOMAS Thematic Conference on the Mechanical Response of Composites, 2013.

[36] Hexcel Composites. HexFlow RTM 6 product data sheet, publication ITA 065 MY18 2017.

[37] Kastner J, Plank B, Salaberger D, Sekelja J. Defect and porosity determination of fibre

reinforced polymers by X-ray computed tomography. 2nd International Symposium on NDT in Aerospace, 2010.